PROCEEDINGS of the
23rd International Congress on Acoustics

9 to 13 September 2019 in Aachen, Germany

Measurement of the structural intensity of curved shell structures by means of 3D laser vibrometry

Nikolai KLEINFELLER[1]; Joachim BÖS[2]; Tobias MELZ[3]

[1,2] System Reliability, Adaptive Structures, and Machine Acoustics SAM, TU Darmstadt, Germany

[3] Fraunhofer Institute for Structural Durability and System Reliability LBF, Germany

ABSTRACT

The structural intensity describes the energy flow of structure-borne sound within a vibrating structure. For complex structures, the STI is usually obtained from a finite element analysis. At the present time, if structures with arbitrary shapes are considered a measurement procedure for validation purposes is not sufficiently developed. For this reason, a measurement procedure for determining the STI of arbitrarily shaped thin-walled structures is developed within the framework of this research project. This paper deals with the measurement of the STI of a curved shell structure by means of 3D laser vibrometry. Therefore, a measurement procedure is set up that consists of measurement data acquisition, measurement data processing, and a general STI calculation. In this context, the challenges of the measurement procedure should be emphasized, if the structures are not flat but curved. In addition to the flexural vibrations, the extensional vibrations must also be recorded simultaneously. In the case of curved structures, knowledge of the curvature properties is necessary in addition to the structural vibrations. Finally, the results are compared to the STI obtained from the virtual data of a finite element analysis.

Keywords: structural intensity, 3D scanning laser vibrometry, thin-walled shell structures

1. INTRODUCTION

The structural intensity (STI) characterizes the energy propagation of structure-borne sound within a vibrating structure (1). In this way transmission paths of structure-borne sound can be analyzed and influenced by structural modifications, e. g., additional masses, to reduce sound radiation at specific frequencies (2). A study has also shown a strong relation between STI-based scalars and the sound radiation of a plate-rip model (3). Thus, the STI can also be used to rate the value of structural modifications compared to an initial state. If the structure is complex, e. g., an oil pan, the STI is usually obtained from a finite element (FE) analysis (2). Consequently, an experimental validation of the STI is a mandatory step if meaningful decisions should be made for structural design.

In the last decades the measurement of STI has mainly been done for straight beams, e. g., (4, 5) or flat plates, e. g., (6, 7). Only a few papers show results of measuring STI of beams and shells with one-dimensional constant curvature, e. g., (8–12). Usually, the progress was delayed by the limitations of the measurement equipment used. In recent years, new measurement techniques have been developed that allow the recording of three-dimensional vibrations with high accuracy. So it is possible to obtain the STI of arbitrarily shaped structures from measurement data. Except from some recently published results by Pires et al. (13) the STI has never been measured for structures with arbitrary shape. Pires et al. (13) used a FE approach for the STI calculation and the digital image correlation (DIC) for the measurement data acquisition. Further, Pires et al. (14) published an alternative measurement strategy for STI based on the shell theory by considering curvature properties. A similar approach is used in this study and has already been tested for a curved beam structure (15).

Therefore, the aim of this paper is the application of the measurement procedure to a curved shell structure. The methodology for determining the STI in curved shells can be divided into three steps as shown in Figure 1.

[1] kleinfeller@sam.tu-darmstadt.de
[2] boes@sam.tu-darmstadt.de (now with Fraunhofer IDMT, joachim.boes@idmt.fraunhofer.de)
[3] info@sam.tu-darmstadt.de

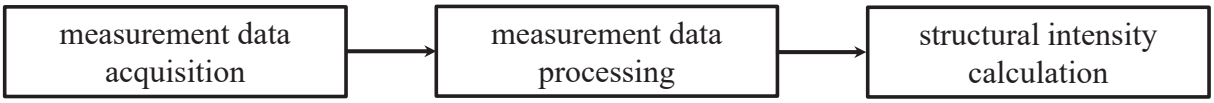

Figure 1 – Measurement procedure for the STI

In the first step the measurement data are recorded by means of a 3D scanning laser vibrometer. In the second step methods of signal processing are used to minimize noise and enable spatial derivative calculation out of measurement data. Finally, the STI is calculated based on a general STI formulation with defined assumptions. The method is applied to a thin-walled and curved shell structure.

The paper is structured as follows. In Section 2, the test specimen as well as the measurement setup and the numerical modelling concept are introduced. A general formulation of the STI for arbitrarily shaped shells is presented in Section 3. In Section 4, the methods of the measurement data processing are described. The results for the STI calculation from measurement data are discussed in Section 5. Section 6 gives a summary and a conclusion.

2. DESIGN OF EXPERIMENTAL AND NUMERICAL MODEL

The measurement procedure for the STI is validated based on a thin-walled spherical shell structure. First, an experimental and a numerical model are built up and are introduced in this section. In this paper the results obtained from the numerical model are called virtual data whereas results from the experimental model are called real measurement data.

2.1 Geometry

Figure 2a shows the geometry of the spherical shell structure considered. The shell structure is made out of steel and was manufactured by a hydroforming process at the Institute of Production Engineering and Forming Machines (PTU) at TU Darmstadt (16). The design parameters are listed in Table 1.

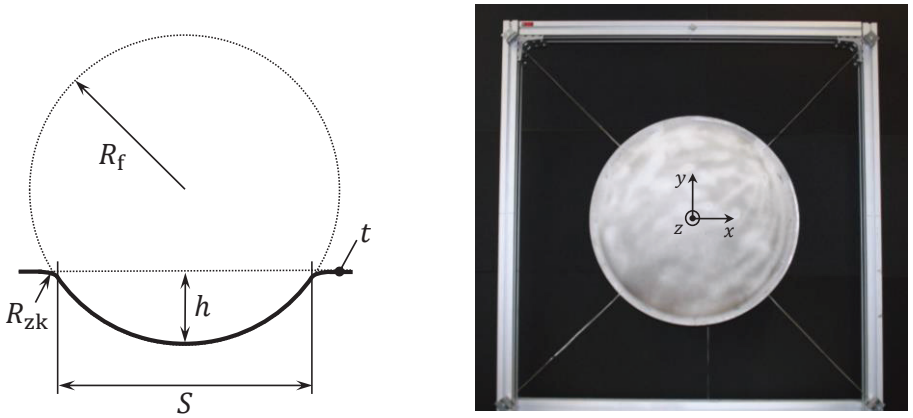

Figure 2 – Curved thin-walled shell structure; a) design parameters (16); b) experimental setup

2.2 Experimental setup

All the measurements were taken at an experimental setup shown in Figure 2b. The test specimen is attached by wires to a frame to achieve free boundary conditions. For harmonic excitation an electrodynamic shaker with a premounted impedance head is used. The measurement data acquisition is done by a 3D scanning laser vibrometer (Polytec PSV-500-3D). So, a simultaneous and complete measurement data acquisition of the three-dimensional structural vibrations (u_x, u_y, u_z) of the shell as well as a measurement of scan point coordinates (x, y, z) is done. The calibration of the laser vibrometer has been done with a high accuracy (<0.2 mm) of the 3D-alignment. First, the vibrations are recorded on a coarse grid using periodic chirp excitation. In this way, the resonance frequencies of the structure are identified. Next, the structure is excited at specific single resonance frequencies. Here, a refined circular measurement grid with a scan points distance of approximately 8 mm in global x-direction as well as in global y-direction is used. This leads to a total number of scan points of 3201

for the complete surface of the spherical shell structure. For every scan point a complex averaging is done over 16 measurements using the excitation force as the reference signal.

Table 1 – design parameters of the curved thin-walled shell structure

parameter	nomenclature	value	unit
diameter	S	620	mm
height	h	66.8	mm
radius	R_{f}	750	mm
radius	R_{zk}	35	mm
thickness	t	1	mm
Youngs's modulus	E	$2.1 \cdot 10^{11}$	N/m^2
Poissons's ratio	ν	0.3	
mass density	ρ	7850	kg/m^3

2.3 Numerical modelling

The shell structure is built up in ANSYS 19.2 by using eight-node shell elements (SHELL281). The wires and the electrodynamic shaker are considered in the model by stiffness (COMBIN14) and mass properties (MASS21). Subsequently, a model-updating is performed. Based on the scanning vibrometer measurements the model parameters are changed to reduce the derivations of the numerical model in relation to the experimental model. This procedure leads to a maximum deviation of 2% for resonance frequencies up to 500 Hz. Further, the structural loss factor ($\eta = 2 \cdot 10^{-4}$) is identified using the 3 dB interpolation method. The model is excited by a discrete excitation force ($F = 0.14$ N). In this way a sufficient agreement between the results of the numerical model and measured displacements is achieved. Figure 3 shows a comparison of magnitude and phase between the simulated (a–d) and the measured (e–h) displacements at a resonance frequency of 209 Hz. On the left hand side (a, b and e, f) are the displacements in global x-direction u_x and on the right hand side (c, d and g, h) are the displacements u_z in global z-direction. The following conclusions can be drawn. First, there is an angular rotation between the results of both models, which can especially be seen from the magnitude of u_z (c and g). Second, the amplitudes of the experimental model are approximately six times higher than the amplitudes of the numerical model. It should be noted that for the study in this paper a qualitative agreement is sufficient. Here, the results of u_z show a qualitatively good agreement between the numerical and the experimental model.

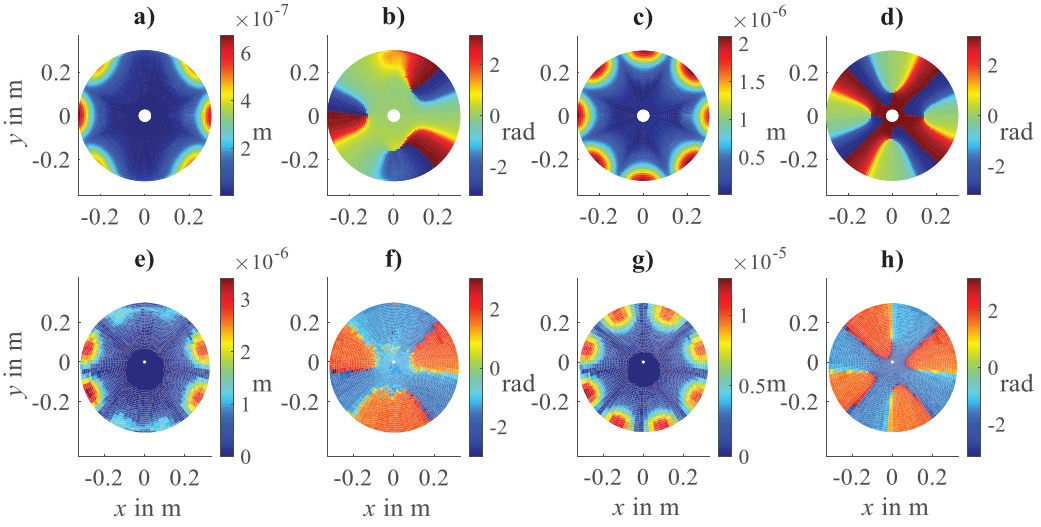

Figure 3 – Magnitude and phase of displacements u_x and u_z; a–d virtual data; e–h measurement data

In contrast, the displacements u_x show major deviations. The results of u_y are similar to u_x so they are not shown here. Summarized, the agreement is sufficient so that the virtual data as well as the real measurement data are taken to obtain the STI based on equations described in Section 3.

3. STRUCTURAL INTENSITY OF SHELLS

A formulation of the STI in thin-walled shells with arbitrary shape was published by Pavić (17) for the first time. The approach is based on the theory of thin shells, which is explained in detail by Qatu (18) and Ventsel and Krauthammer (19). Generally, the spatial intensity vector (1)

$$\boldsymbol{I} = \left[I_x, I_y, I_z\right]^T = -\boldsymbol{S} \cdot \boldsymbol{v} \tag{1}$$

is calculated from the product of the stress tensor $\boldsymbol{S}$ and the vibrational velocity $\boldsymbol{v}$. Equation 1 is valid for any elastic medium. In the case of thin-walled structures, the component of the STI in thickness direction can be neglected ($I_z \approx 0$). If the shell has an arbitrary shape, it is useful to define a new local coordinate system (α, β, γ) that is curvilinear and body-fitted and makes mathematical operations easier to perform (17–19). The resulting intensity at the shell's middle surface

$$I' = \int_{-t/2}^{+t/2} \boldsymbol{I}\ \mathrm{d}z = \begin{bmatrix} I'_\alpha \\ I'_\beta \end{bmatrix} = -\begin{bmatrix} N_\alpha \dot{u}_\alpha + N_{\alpha\beta}\dot{u}_\beta + M_\alpha \dot{\lambda}_\alpha + M_{\alpha\beta}\dot{\lambda}_\beta + Q_\alpha \dot{u}_\gamma \\ N_\beta \dot{u}_\beta + N_{\beta\alpha}\dot{u}_\alpha + M_\beta \dot{\lambda}_\beta + M_{\beta\alpha}\dot{\lambda}_\alpha + Q_\beta \dot{u}_\gamma \end{bmatrix} \tag{2}$$

can be obtained by integrating the intensity vector across the shell thickness t. The internal forces and moments of an arbitrary shell in Equation 2 are defined as (17–19)

$$\begin{aligned}
N_{\alpha,\beta} &= \frac{Et}{1-\nu^2}\left(\varepsilon_{\alpha,\beta} + \nu\varepsilon_{\beta,\alpha}\right), \\
N_{\alpha\beta,\beta\alpha} &= \frac{Et}{2(1+\nu)}\varepsilon_{\alpha\beta,\beta\alpha}, \\
M_{\alpha,\beta} &= \frac{Et^3}{12(1-\nu^2)}\left(\kappa_{\alpha,\beta} + \nu\kappa_{\beta,\alpha}\right), \\
M_{\alpha\beta,\beta\alpha} &= \frac{Et^3}{24(1+\nu)}\kappa_{\alpha\beta,\beta\alpha}, \\
Q_\alpha &= \frac{1}{AB}\left[\frac{\partial}{\partial\alpha}(BM_\alpha) - \frac{\partial B}{\partial\alpha}M_\beta + \frac{1}{A}\frac{\partial}{\partial\beta}\left(A^2 M_{\alpha\beta}\right)\right], \\
Q_\beta &= \frac{1}{AB}\left[\frac{\partial}{\partial\beta}\left(AM_\beta\right) - \frac{\partial A}{\partial\beta}M_\alpha + \frac{1}{B}\frac{\partial}{\partial\alpha}\left(B^2 M_{\beta\alpha}\right)\right].
\end{aligned} \tag{3}$$

In this case the kinematics of the shells are described by the Kirchhoff's assumptions. Furthermore, the material properties are assumed to be linear and isotropic. The midsurface strains (ε_α, ε_β, $\varepsilon_{\alpha\beta}$, $\varepsilon_{\beta\alpha}$), curvatures and twist (κ_α, κ_β, $\kappa_{\alpha\beta}$) as well as rotations (λ_α, λ_β) are obtained from

$$\begin{aligned}
\varepsilon_\alpha &= \frac{1}{A}\frac{\partial u_\alpha}{\partial\alpha} + \frac{1}{AB}\frac{\partial A}{\partial\beta}u_\beta + \frac{u_\gamma}{R_1}, \\
\varepsilon_\beta &= \frac{1}{B}\frac{\partial u_\beta}{\partial\beta} + \frac{1}{AB}\frac{\partial B}{\partial\alpha}u_\alpha + \frac{u_\gamma}{R_2}, \\
\varepsilon_{\alpha\beta} = \varepsilon_{\beta\alpha} &= \frac{B}{A}\frac{\partial}{\partial\alpha}\left(\frac{u_\beta}{B}\right) + \frac{A}{B}\frac{\partial}{\partial\beta}\left(\frac{u_\alpha}{A}\right), \\
\kappa_\alpha &= \frac{1}{A}\frac{\partial\lambda_\alpha}{\partial\alpha} + \frac{1}{AB}\frac{\partial A}{\partial\beta}\lambda_\beta, \\
\kappa_\beta &= \frac{1}{B}\frac{\partial\lambda_\beta}{\partial\beta} + \frac{1}{AB}\frac{\partial B}{\partial\alpha}\lambda_\alpha,
\end{aligned} \tag{4}$$

$$\kappa_{\alpha\beta} = \frac{B}{A}\frac{\partial}{\partial\alpha}\left(\frac{\lambda_\beta}{B}\right) + \frac{A}{B}\frac{\partial}{\partial\beta}\left(\frac{\lambda_\alpha}{A}\right),$$

$$\lambda_\alpha = \frac{u_\alpha}{R_1} - \frac{1}{A}\frac{\partial u_\gamma}{\partial\alpha},$$

$$\lambda_\beta = \frac{u_\beta}{R_2} - \frac{1}{B}\frac{\partial u_\gamma}{\partial\beta}.$$

Therefore, the displacements of the midsurface in the local curvilinear coordinate system (u_α, u_β, u_γ) as well as their spatial derivatives are necessary. A and B are called the Lamé parameters of the surface. The Lamé parameters are obtained from (17, 19)

$$A, B = \sqrt{{x^2}_{\alpha,\beta} + {y^2}_{\alpha,\beta} + {z^2}_{\alpha,\beta}} \tag{5}$$

with the derivative of the scan point coordinates with respect to the local coordinate directions α and β. Further, R_1 and R_2 are the radii of principal curvature and are related to the change in direction of the normal vectors of the surface. The determination of principal curvatures based on discrete coordinate data is explained by (17, 19) and will not be described here. In this study a spherical shell is considered, which leads to equal principal curvatures at any point on the surface. If monofrequent steady-state signals are assumed, the complex STI $\underline{\boldsymbol{I}}(f)$ in the frequency domain yields

$$\underline{\boldsymbol{I}}(f) = -\frac{1}{2}\cdot\underline{\boldsymbol{S}}(f)\cdot\underline{\boldsymbol{v}}^*(f) \tag{6}$$

by using peak values of the complex stress tensor $\underline{\boldsymbol{S}}$ and the conjugate complex vibrational velocity $\underline{\boldsymbol{v}}^*$. The real part of the complex STI, $\boldsymbol{I}_\mathrm{a} = \mathrm{Re}\{\underline{\boldsymbol{I}}(f)\}$, is called active STI, whereas the imaginary part of the complex STI, $\boldsymbol{I}_\mathrm{r} = \mathrm{Im}\{\underline{\boldsymbol{I}}(f)\}$, is called reactive STI. In the framework of this paper the STI is always analyzed in the frequency domain.

4. MEASUREMENT DATA PROCESSING

It is shown in Section 3 that the STI can be calculated based on measured discrete three-dimensional vibrations and on related scan point coordinates. Thus, a measurement procedure is tested by using real measurement data recorded by a 3D scanning laser vibrometer. The measurement procedure shown here has also been published by Pires et al. (14). The approach is based on a complete and general description of the STI in a thin-walled shell structure, see Equations 2–4. The entire STI can be obtained for the grid of defined scan points if the coordinates with respect to a global measurement coordinate system (x, y, z) as well as the three-dimensional structural vibrations (u_x, u_y, u_z) are known. The complete measurement procedure is verified by using virtual data obtained from an FE analysis.

Measured data of three-dimensional vibrations and coordinates must be filtered to reduce noise. Here, a spatial filter of the Polytec Strain Processor (PSV 9.3) is used, which produced satisfactory results. An alternative approach can be a Savitzky-Golay filter (20) used frequently for dynamic strain measurements, e. g., by Wildy (21).

Subsequently, the spatial derivatives of the local displacements are obtained from the data. In the first step, a local curvilinear coordinate system must be identified for each scan point. This can be done by calculating the tangential vectors with respect to the α- and β-direction for each scan point and assuming that the direction of vectors fits with the direction of a local curvilinear coordinate system. If the local vector base is known, the related transformation matrix is calculated. Additionally, the curvature properties of the underlying shell surface are obtained. The left hand side of Figure 4 (a, b and e, f) shows a selection from two out of nine transformation coefficients calculated by virtual coordinates (a, b) and measured scan point coordinates (e, f). In the first case (a and e) a quantitative agreement is achieved except for single deviations located around the circle center. In the second case (b and f) results are worse. The deviations are caused due to noise of the scan point coordinate measurement data. Summarized, over all nine transformation coefficients a qualitative agreement is achieved.

In the next step, the measured three-dimensional vibrations are transformed to the local coordinate systems by using the transformations calculated before. Subsequently, the derivatives of the local structural vibrations up to the third order are calculated. For the calculation of the spatial derivatives the finite difference scheme is applied. So, the first order spatial derivate of a scan point with number i, e .g., of the displacement in α-direction, is obtained from

$$\left(\frac{\partial u_\alpha}{\partial \alpha}\right)_i \approx \frac{u_{\alpha,i+1} - u_{\alpha,i-1}}{\Delta s}. \tag{7}$$

Here, $u_{\alpha,i+1}$, $u_{\alpha,i-1}$ are the displacements values of neighbor points and Δs is the scan point distance obtained from the magnitude of the distance vector between two scan points. For higher order derivatives an equal scheme is used. For scan points close to the boundary, a forward or backwards finite difference scheme is applied. Figure 4 (c, d and g, h) shows a comparison between calculated first order spatial derivatives of u_γ with respect to α-direction from virtual data (c and d) and from measurement data (g and h). Here, a qualitative agreement is also achieved if the results of Section 2.3 are taken into account. It should be mentioned at this point that the results for the first order displacements u_α and u_β are worse. This fact can be explained by phase noise occurred due to measurement deviations. Finally, after having obtained the higher order derivatives as well, the STI is calculated with respect to the local coordinate system. Subsequently, the STI with respect to the global coordinate system is obtained from inverse transformation.

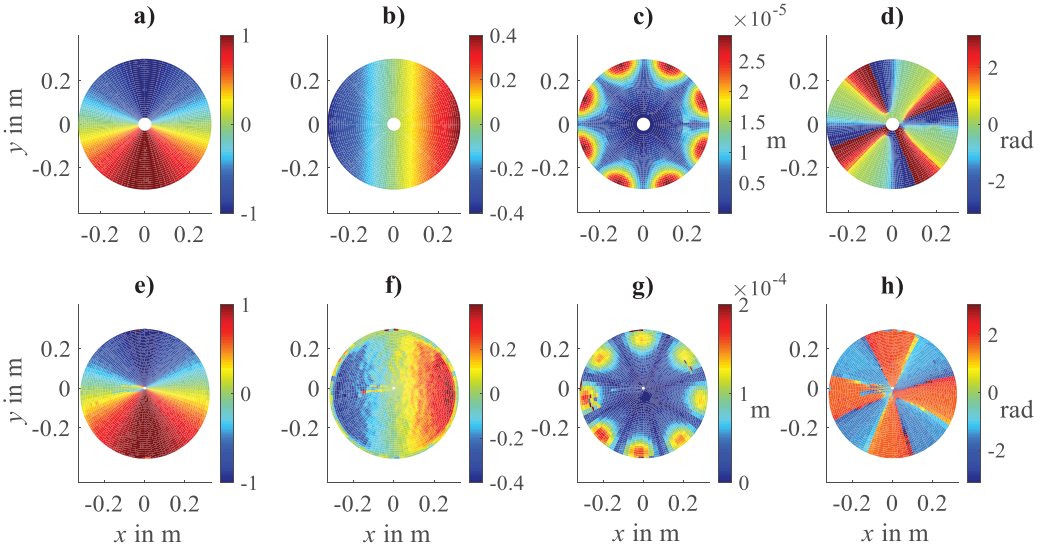

Figure 4 – Transformation coefficients and magnitude and phase of the first order spatial derivative of u_γ; a–d virtual data; e–h measurement data

5. RESULTS OF THE STUDY

In this section the active and reactive STI calculated from measurement data are compared with the STI obtained from virtual data. The STI is composed of four parts (bending moment, twisting moment, shear force and membrane force). Figure 5 shows the results of the active and reactive intensities of the bending moment calculated by using virtual data (a, b) and real measurement data (c, d). For visualization purposes the STI is only shown in a section of the surface. The magnitude of the STI is visualized as a contour plot and the spatial STI vectors are displayed as white arrows. It should be noted that at specific spots of the surface a deterioration of the measurement results occurs due to measurement deviations. Figure 6 visualizes the results of the active and reactive intensities of the twisting moment. On the one hand, there is a qualitatively good agreement between the spatial distribution of the STI magnitude for both the bending moment and the twisting moment. On the other hand, the direction of the STI vectors is clearly defined. Even though a change in direction occurs for active STI the transmission paths are identifiable. Summing up the results, it can be concluded that for the bending moment and the twisting moment the measurement procedure is reliable enough and a sufficient agreement has been achieved. In contrast, the results for the STI of the shear forces are

not usable due to distortions by measurement errors. A successful calculation of intensities due to membrane forces from measurement data can also not be achieved in this study. In comparison to flat structures the STI calculation of curved structures is affected by calculation errors resulting from coupling of up to six measurement quantities and their spatial derivatives if the method proposed in this paper is used. In this study the results are strongly influenced by deviations of the scan point coordinate measurement data. Further investigations will focus on improving the measurement procedure by implementing additional data filters, e.g. using Savitzky-Golay filter (20).

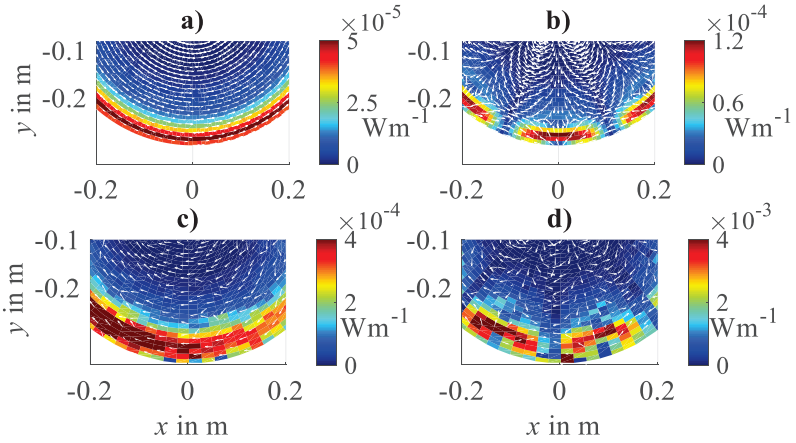

Figure 5 – $\boldsymbol{I}_{\mathrm{a}}$ and $\boldsymbol{I}_{\mathrm{r}}$ of the bending moment; a–b virtual data; c–d measurement data

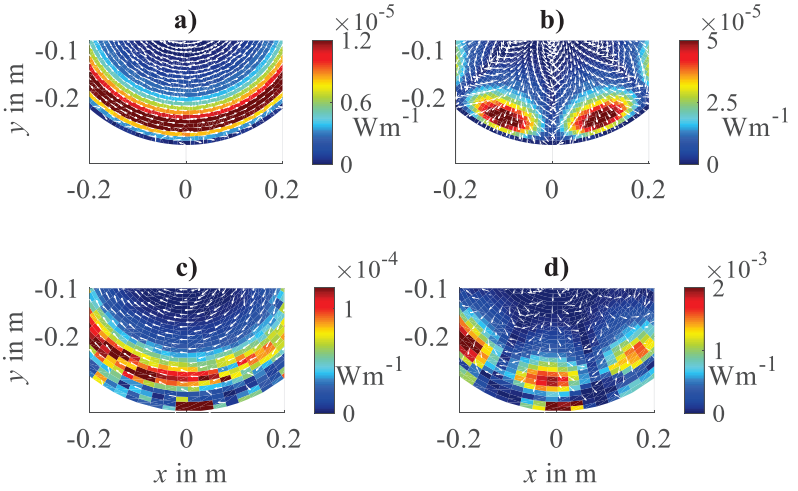

Figure 6 – $\boldsymbol{I}_{\mathrm{a}}$ and $\boldsymbol{I}_{\mathrm{r}}$ of the twisting moment; a–b virtual data; c–d measurement data

6. SUMMARY AND CONCLUSIONS

This paper presents a measurement procedure for determining the STI in curved shell structures. In this context, a spherical shell structure is used as a test specimen. In the first step, the structural vibrations and the scan point coordinates are recorded by a 3D scanning laser vibrometer. In the second step, the coordinate transformations and the spatial derivatives of the displacements with respect to a local curvilinear coordinate system are calculated. Finally, the STI is obtained by equations based on the shell theory by considering curvature properties.

It is found that the results show a sufficient agreement if the STI for the bending moment and the twisting moment are of interest. A measurement of the STI for the shear forces and the membrane forces has not been successful especially due to measurement deviations of scan point coordinates. Future work will involve the enabling of the STI measurements for the membrane and the shear forces due to improvements in the measurement data processing. Finally, the method will be applied to a more complex structure, e. g., an oil pan.

ACKNOWLEDGEMENTS

The authors appreciate the contributions of the student Xiang Liu to this research project. The project is funded by the Deutsche Forschungsgemeinschaft DFG (BO 3624/1-1 and INST 163/520-1 FUGG). This funding is gratefully acknowledged.

REFERENCES

1. Pavić G. Structure-borne energy flow. In: Handbook of noise and vibration control (ed. M. J. Crocker), John Wiley & Sons, Inc., Hoboken, New Jersey, USA, 2007, pp. 232–240.
2. Hering T. Strukturintensität als Werkzeug der Maschinenakustik (Structural intensity analysis as a tool for engineering noise control), PhD Thesis, TU Darmstadt, Germany, 2012.
3. Schaal C, Ebert J, Bös J, Melz T. Relation between structural intensity-based scalars and sound radiation using the example of plate-rib model, ASME Journal of Vibration and Acoustics, 2016, 138(4): pp. 041011–1–041011–9.
4. Hambric S A, Taylor P D. Comparison of experimental and finite element structure-borne flexural power measurements for a straight beam. Journal of Sound and Vibration, 1994, 170(5): pp. 595–605.
5. Audrain P, Masson P, Berry A. Investigation of active structural intensity control in finite beams: Theory and experiment. Journal of the Acoustical Society of America, 2000, 108(2): pp. 612–623.
6. Blotter J D, West R L, Sommerfeldt S D. Spatially continuous power flow using a scanning laser Doppler vibrometer. ASME Journal of Vibration and Acoustics, 2002, 124(4): pp. 476–482.
7. Pascal J C, Carniel X, Li J F. Characterization of a dissipative assembly using structural intensity measurements and energy conservation equation. Mechanical Systems and Signal Processing, 2006, 20(6): pp. 1300–1311.
8. Walsh S J, White R G. Vibrational power flow transmission in curved beams, Journal of Sound and Vibration, 2000, 233(3): pp. 455–488.
9. Walsh S J, White R G. Measurement of vibrational power transmission in curved beams, Journal of Sound and Vibration, 2001, 241(2): pp. 157–183.
10. Williams E G. Structural intensity in thin cylindrical shells. Journal of the Acoustical Society of America, 1991, 89(4): pp. 1615–1622.
11. Saijyou K, Yoshikawa S. Structural intensity measurement of cylindrical shell based on NAH technique and influences of a rib on the acoustic energy flow. Journal of Acoustical Society of Japan, 1999, 20(2): pp. 125–136.
12. Salimi-Mofrad H, Ziaei-Rad S, Moradi M. Vibrational power flow analysis of a cylindrical shell using a four-point technique. International Journal of Acoustics and Vibration, 2014, 19(2): pp. 127–130.
13. Pires F, Avirl S, Vanlanduit S, Dirckx J J J. Structural intensity assessment on shells via a finite element approximation, Journal of the Acoustical Society of America, 2019, 145(1): pp. 312–326.
14. Pires F, Vanlanduit S, Dirckx J J J. Structural intensity analysis on irregular shells, ASME Journal of Vibration and Acoustics, 2019, 141(1): pp. 011011–1–011011–12.
15. Kleinfeller N, Bös J, Melz T. Entwicklung eines Messverfahrens zur Bestimmung der Strukturintensität von dünnwandigen und gekrümmten Strukturen (Development of a measurement procedure for determining the structural intensity of thin-walled and curved structures). Proc 45th Annual German Conference on Acoustics – DAGA 2019, 18–21 March 2019, Rostock, Germany, pp. 1022–1025.
16. Bäcker F. Formgebung mehrachsig stark gekrümmter Stahlbleche mit lastangepassten Versteifungsrippen (Shape of multiaxial strongly curved steel sheets with load-adapted stiffening rips). PhD Thesis, TU Darmstadt, Germany, 2015.
17. Pavić G. Vibrational energy flow in thin-walled shells, Proc 3rd International Congress on Intensity Techniques, 27–29 August 1990, Senlis, France, pp. 91–96.
18. Qatu M S. Vibration of laminated shells and plates. Elsevier Ltd., Amsterdam, The Netherlands, 2004.
19. Ventsel E, Krauthammer T. Thin plates and shells: Theory, Analysis and Application, Marcel Dekker, New York, USA, 2001.
20. Savitzky A, Golay M J. Smoothing and differentiation of data by simplified least-squares procedures, Analytical Chemistry, 1964, 36(8): pp. 1627–1639.
21. Wildy S. Scanning laser doppler vibrometry for strain measurement and damage detection. PhD Thesis, The University of Adelaide, Australia, 2012